

Document downloaded from:

<http://hdl.handle.net/10251/147994>

This paper must be cited as:

Gil-Castell, O.; Badia, J.; Strömberg, E.; Karlsson, S.; Ribes-Greus, A. (2017). Effect of the dissolution time into an acid hydrolytic solvent to taylor electrospun nanofibrous polycaprolactone scaffolds. *European Polymer Journal*. 87:174-187.
<https://doi.org/10.1016/j.eurpolymj.2016.12.005>



The final publication is available at

<https://doi.org/10.1016/j.eurpolymj.2016.12.005>

Copyright Elsevier

Additional Information

**EFFECT OF THE DISSOLUTION TIME INTO AN ACID
HYDROLYTIC SOLVENT TO TAYLOR ELECTROSPUN
NANOFIBROUS POLYCAPROLACTONE SCAFFOLDS**

O. Gil-Castell¹, J. D. Badia^{1,2,3}, E. Strömberg⁴, S. Karlsson^{4,5}, A. Ribes-Greus^{1,*}.

¹Instituto de Tecnología de Materiales (ITM).
Universitat Politècnica de València.
Camino de Vera s/n, 46022 Valencia, Spain.

² Departament de Química Orgànica i Analítica,
Universitat Rovira i Virgili,
C/Marcel·lí Domingo s/n, 43007 Tarragona, Spain.

³ Departament d'Enginyeria Química,
Escola Tècnica Superior d'Enginyeria, Universitat de València,
Avinguda de la Universitat s/n, 46100 Burjassot, Spain.

⁴KTH Royal Institute of Technology,
School of Chemical Science and Engineering,
Fibre and Polymer Technology,
Teknikringen 56-58, SE-10044 Stockholm, Sweden.

⁵Skövde University,
SE-541 28 Skövde, Sweden

*Corresponding author:
A. Ribes-Greus
aribes@ter.upv.es
Tel. 0034 630125695

EFFECT OF THE DISSOLUTION TIME INTO AN ACID HYDROLYTIC SOLVENT TO TAYLOR ELECTROSPUN NANOFIBROUS POLYCAPROLACTONE SCAFFOLDS

O. Gil-Castell¹, J. D. Badia^{1,2,3}, E. Strömberg⁴, S. Karlsson^{4,5}, A. Ribes-Greus^{1,*}.

Abstract

The hydrolysis of the polycaprolactone (PCL) as a function of the dissolution time in a formic/acetic acid mixture was considered as a method for tailoring the morphology of nanofibrous PCL scaffolds. Hence, the aim of this research was to establish a correlation between the dissolution time of the polymer in the acid solvent with the physico-chemical properties of the electrospun nanofibrous scaffolds and their further service life behaviour.

The physico-chemical properties of the scaffolds were assessed in terms of fibre morphology, molar mass and thermal behaviour. A reduction of the molar mass and the lamellar thickness as well as an increase of the crystallinity degree were observed as a function of dissolution time. Bead-free fibres were found after 24 and 48 h of dissolution time, with similar diameter distributions. The decrease of the fibre diameter distributions along with the apparition of beads was especially significant for scaffolds prepared after 72 h and 120 h of dissolution time in the acid mixture.

The service life of the obtained devices was evaluated by means of *in vitro* validation under abiotic physiological conditions. All the scaffolds maintained the nanofibrous structure after 100 days of immersion in water and PBS. The molar mass was barely affected and the crystallinity degree and the lamellar thickness increased along immersion, preventing scaffolds from degradation. Scaffolds prepared after 24 h and 48 h kept their fibre diameters, whereas those prepared after 72 h and 120 h showed a significant reduction.

This PCL tailoring procedure to obtain scaffolds that maintain the nanoscaled structure after such long *in vitro* evaluation will bring new opportunities in the design of long-term biomedical patches.

Keywords

Electrospinning, scaffold, hydrolysis, polycaprolactone (PCL), *in vitro* validation

1. Introduction

The development of scaffolds for biomedical applications is focused on the fabrication of biological substitutes that restore, maintain or improve either a particular tissue or even an entire organ, through an adequate cell adhesion and proliferation procedure. These nanoscaled scaffolds mimic extracellular matrix (ECM) which is known to play a key role in tissue regeneration field [1] [2].

Electrospinning is one of the most applied methods for polymer-based fibrous devices production in the nanoscale range. This technique permits the fabrication of non-woven nanomats with large surface area-to-volume ratio and high porosity, which have found interesting applications in the biomedical sector [3] [4] [5] [6] [7]. The electrospinning process is based on the application of a high voltage electric field between the tip of a syringe and a collector to transform a polymer solution into mats of non-woven nanofibres [8] [9] [10] [11] [12]. The suitability of this process is known to depend on the synergistic effect of the solution and processing conditions [13] [14]. Indeed, some difficulties during the preparation of the scaffolds propitiated a field of interest.

A variety of natural and synthetic polymers have been widely used for scaffold fabrication such as poly(lactic acid) (PLA), poly(lactic-co-glycolic acid) (PLGA) or poly(caprolactone) (PCL), with diverse applications according to their durability when subjected to service life conditions [9] [11]. Among these, PCL is a semicrystalline linear aliphatic polyester that is widely applied in biomedicine due to its biocompatibility and slow biodegradability. PCL has been validated both *in vitro* and *in vivo* in the biomedical sector for long-term applications [15] [16] [17] [18] [19] [20] [21] [22] [23] [24] [25] [26] [27] [28]. However, producing electrospun bead-free fibres of PCL in the nanoscale range has become a delicate issue which has been tried to overcome [29] [30] [31] [32] [33] [34] [35] [36]. This is the reason why highly toxic solvents such as chloroform, dimethylformamide, methylene chloride or dichloroethane have been required for the electrospinning of PCL [37] [38] [39].

Several alternative solvents have been recently proposed for the electrospinning of PCL, with the aim of reducing the exposure of technicians to toxic solvents [40]. Acetone was appointed by Bosworth et al. with promising results [41]. Bisnual et al. produced nanofiber scaffolds via electrospinning of PCL using diluted acetic acid-ethyl acetate for bone tissue engineering [42]. Van der Schueren et al. found an innovative solvent mixture of formic/acetic acid with an effective nanofiber fabrication under steady-state conditions [43]. Although hydrolytic degradation of PCL through cleavage of the ester bond occurs in the aqueous acidic media, it was shown that the viscosity of a PCL solution in formic/acetic acid was high enough for suitable electrospinning in steady-state conditions [43] [44] [45]. Lavielle et al. studied the formation of PCL electrospun fibres in this acidic medium and modelled the loss of molar mass as a function

of the time of dissolution of the polymer in the solution [44]. Taking these references as a baseline for this research, it seems therefore interesting to extend these studies to tailor the structure and physico-chemical performance of electrospun nanofibrous scaffolds as a function of the dissolution time of PCL in the acid solvent, which will determine its subsequent behaviour during its application [14, 29, 33, 46, 47, 48]. Literature propose that properties such as the fibre morphology, the molar mass, the crystallinity degree or the lamellar thickness play an important influence during the application of a biodegradable biomedical device, as studied for some polyesters such as PLA or PCL [19, 47, 48, 49]. Indeed, by adopting a particular fibre morphology (i.e. size scale) and mode of assembly of polymer chains (i.e. crystallinity), it is possible to influence the cell adhesion and proliferation kinetics, and further determine the course of their differentiation process [14]. During application, the rate of biodegradation is also a crucial aspect, determined by the accessibility of water to the ester bonds, which is affected by a number of factors such as the hydrophobicity of the monomer, the crystallinity of the sample, the molar mass or the bulk sample dimensions, among others [50] [51] [52]. Due to the reported higher degradation rate of amorphous regions versus that of the crystalline ones, the crystallinity degree is one of the most dominant factors. Actually, the effect of the molar mass on the crystallisation kinetics of PCL has been previously reported by Jenkins and Harrison [48]. As a consequence, a deep characterisation based on the morphology, the molar mass and the microstructure as well as the *in vitro* validation as a function of the time of dissolution of the polymer into the hydrolytic acid solvent is essentially required.

The aim of this research was therefore to establish a correlation between the dissolution time of the PCL in the hydrolytic solvent system based on formic/acetic acid (1:1) and its resultant structure, physico-chemical properties and further *in vitro* performance.

2. Materials and methods

2.1. Materials

Polycaprolactone (PCL) was provided by Perstorp as 3 mm diameter pellets under the CAPA™ 6800 grade ($M_n = 85000 \text{ g}\cdot\text{mol}^{-1}$ and T_m 58-60 °C). Formic acid and acetic acid ($\geq 99\%$) were used as solvents for electrospinning. Tetrahydrofuran (THF) ($\geq 99.8\%$) was used as solvent for the GPC analyses. Dulbecco's Phosphate Buffer Saline (PBS) and NaOH solution 1 M were used for the *in vitro* validation procedure. All of them were supplied by Sigma-Aldrich and were used without further purification. Ultra-pure water, as obtained from an ultra-filtration/ion-exchange procedure was used for the *in vitro* validation.

2.2. Polymer solution and electrospinning

Electrospinning was performed by means of an horizontal setup composed of a Spellman SL80 high voltage supply, a Thermo Orion Sage® 361 programmable syringe pump, a Normax Ruthe 20 mL Luer Lock glass syringe, silicon tube, and a Luer-Lock gauge 21 metallic needle. The tip-to-collector distance was maintained constant at 12.5 cm. Solutions for electrospinning were prepared in 1:1 formic/acetic acid, with a polymer concentration of 15% wt and were electrospun after 24, 48, 72 and 120 h of dissolution time. Complete dissolution of the polymer was guaranteed after 24 h, whereas after 120 h the viscosity of the solution was excessively low to ensure stable electrospinning. The feeding rate varied between 0.5, 1 and 1.5 mL·h⁻¹ and the voltage varied between 15, 20 and 25 kV. Electrospinning was performed during 30 min at room temperature (22 °C) and 35% of relative humidity. Fibrous scaffolds were collected on aluminium foil, then dried and stored for further analyses.

2.3. Scaffold characterisation

2.3.1. Field-emission scanning electron microscopy (FE-SEM)

The surface topology of the specimens was analysed by means of a Zeiss Ultra 55 field emission scanning electron microscope (FE-SEM). The samples were cut into small pieces and dried at 50 °C in a vacuum oven for 24 h and then kept in a desiccator during 48 h. Afterwards, the specimens were mounted on metal studs and sputter-coated with a platinum layer during 10 s using a Leica EM MED020 sputtering equipment. Testing was performed at room temperature with a 2 kV voltage. The fibre diameters were measured from the FE-SEM micrographs (10000×) at random locations ($n = 100$) with the aid of the Image J software.

2.3.2. Size exclusion chromatography (SEC)

Size exclusion chromatography (SEC) analyses were carried out by means of a Malvern Instruments OMNISEC RESOLVE chromatograph. It combined integrated pump, degasser, autosampler and column oven, along with a Malvern Instruments OMNISEC REVEAL multi-detector –UV, Refractive Index (RI), Low and Right Angle Light Scattering (LALS and RALS) and Viscosity (VISC)–. Two columns from Malvern Instruments (T2000 and T4000) were employed (300×8 mm). The samples were dissolved in THF with concentrations of around 2.0 mg·ml⁻¹ and filtered through 0.45 µm PTFE filters. As well, THF was used as mobile phase at a flow rate of 1 mL·min⁻¹ and the column temperature was set at 35 °C. A monodisperse polystyrene standard with dn/dc value of 0.185 was used for previous calibration. Two injections per sample were performed and the obtained data were analysed by means of the OMNISEC V10™ software.

2.3.3. Fourier transformed infrared spectroscopy (FT-IR)

The determination of the initial composition of the scaffolds as well as the preliminary study of the crystalline morphology was performed via attenuated total reflectance (ATR) in a Thermo Nicolet 5700 Fourier transform infrared spectrometer (FT-IR). The average spectra were collected from 64 scans with a resolution of 4 cm⁻¹ in the 4000-600 cm⁻¹ range, from eight different locations of the same specimen.

2.3.4. Differential scanning calorimetry (DSC)

Calorimetric data were obtained by differential scanning calorimetry by means of a Mettler-Toledo DSC 820^e equipment, previously calibrated following the procedure of In and Zn standards. The samples, with a mass of about 4 mg, were analysed between 0 and 80 °C with a heating/cooling/heating rate of 10 °C·min⁻¹. All experiments were run under nitrogen atmosphere (50 mL·min⁻¹). The specimens were characterised at least by triplicate and the averages of temperatures and enthalpies were taken as representative values.

The crystallinity degree (X_c) was evaluated from the melting enthalpy results, by using **Equation 1**,

$$X_c (\%) = \frac{\Delta h_m}{\Delta h_m^0} \cdot 100 \quad \text{(Equation 1)}$$

where Δh_m is the melting enthalpy of the sample and Δh_m^0 is the melting enthalpy of a perfect crystal of PCL (148 J·g⁻¹) [53] [54] [55] [56].

2.4. In vitro hydrolytic degradation

The electrospun PCL scaffolds were subjected to hydrolytic degradation in ultra-pure water and phosphate buffer solution (PBS), according to the international standard ISO 10993-13:2010, method 4.3 [57]. The pH of the PBS solution was previously adjusted to 7.4 with NaOH 1M. The electrospun scaffolds were cut into rectangular specimens with a mass around 10 mg. The specimens were weighed (m_0) and placed in a previous weighed vial (m_{vial}). 10 mL of degradation medium were introduced and then the vials were sealed with polytetrafluoroethylene (PTFE) threaded plugs and placed in a thermostatically controlled oven at 37 °C. The effects of the hydrolytic degradation were evaluated after 100 days of immersion both in the solid and in the liquid. The liquid fraction was analysed immediately after extraction. The pH of the degradation media was measured at room temperature by using a Crison pH25 device. Three buffer solutions from Crison were used to calibrate the pH-meter: pH 4.01 (phthalate buffer solution), pH 7.00 (phosphate buffer solution), pH 10.01 (borate buffer solution). The remaining solid fraction coming from the saline buffer was washed with deionized water and then, along with specimens

coming from water environment, dried under vacuum to constant mass into their degradation vials (m_{dry}) and saved for further analyses. The mass loss of the specimens was calculated according to **Equation 2**.

$$Mass\ loss\ (\%) = 100 - \frac{(m_{dry} - m_{vial})}{m_0} \cdot 100 \quad \text{(Equation 2)}$$

3. Results and discussion

3.1. Preliminary study of the electrospinning viability

The electrospinning viability was addressed under different experimental conditions: dissolution time of the PCL in the hydrolytic acid solvent (24–120 h), feeding rate ($0.5\text{--}1\text{ mL}\cdot\text{h}^{-1}$) and voltage (15–25 kV), in order to establish the effect of each parameter on the final electrospun scaffolds. Other factors such as the polymer type, solvent type, concentration, needle diameter, tip-to-collector distance, collector type, working time, temperature and humidity remained fixed, as specified in the experimental section. In general terms, the system turned unstable and dripped for low voltages and high feeding rates, while consumption of the material in the tip and unstable Taylor cone was found for high voltages and low feeding rates. **Table 1** gathers the experimental conditions in which electrospinning was viable, which micrographs can be found in **Figure 1**.

Figure 2 shows that the influence of the voltage and the feeding rate on the fibre diameter regardless the dissolution time was not as relevant. Therefore, this study is focused from now onwards on the effect of the dissolution time in the hydrolytic acid solvent from the electrospun scaffolds labelled as 4, 8, 12 and 15, obtained with a feeding rate of $1\text{ mL}\cdot\text{h}^{-1}$ and a voltage of 25 kV.

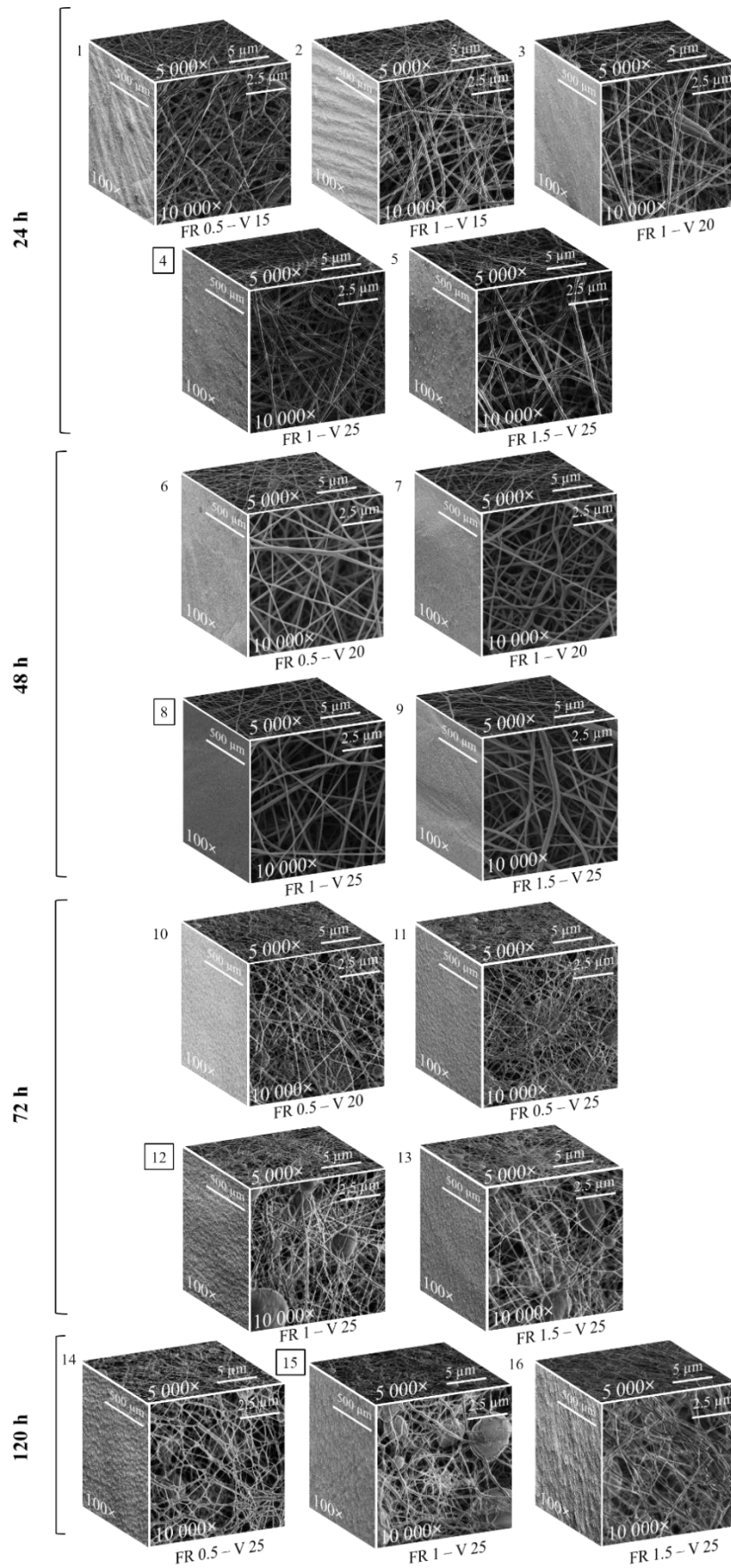


Figure 1. FE-SEM micrographs for the viable electrospinning process as function of dissolution time, feeding rate (FR) and voltage (V) (100, 5 000 and 10 000 \times , 3 kV). (□ Indicate those scaffolds chosen for further characterisation)

Table 1. Electrospinning viability for dissolution time (24, 48, 72 and 120 h), feeding rate (0.5, 1 and 1.5 mL·h⁻¹) and voltage (15, 20 and 25 kV). (✓) Stands for viable, while (–) for unviable conditions. Superindexes are identifiers for the **Figure 1**. (◀ Indicate those specimens chosen for the study)

Dissolution time (h)	Feeding Rate (mL·h ⁻¹)	Voltage (kV)		
		15	20	25
24	0.5	✓ 1□	–	–
	1	✓ 2	✓ 3	✓ 4◀
	1.5	–	–	✓ 5□
48	0.5	–	✓ 6	–
	1	–	✓ 7	✓ 8◀
	1.5	–	–	✓ 9
72	0.5	–	✓ 10□	✓ 11□
	1	–	–	✓ 12◀
	1.5	–	–	✓ 13□□
120	0.5	–	–	✓ 14□□
	1	–	–	✓ 15◀
	1.5	–	–	✓ 16□□

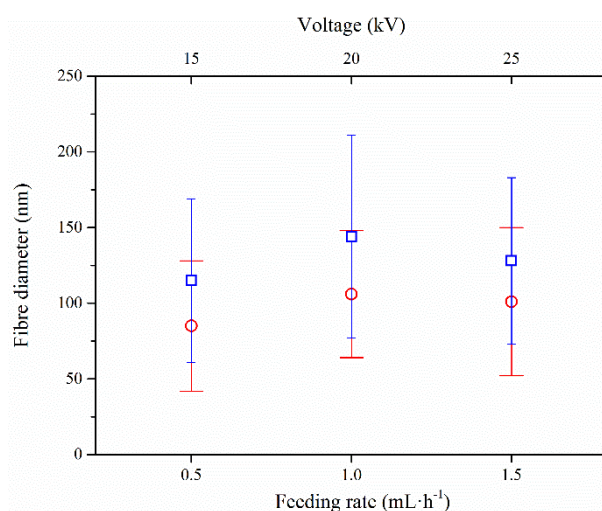


Figure 2. Influence of voltage (V) (square □; DT = 24 h) and influence of feeding rate (FR) (circle ○; DT = 72 h) on scaffold fibre diameter. Mean fibre diameter and standard deviation, as calculated from the FE-SEM micrographs (10000×) at random locations ($n = 100$). DT stands for dissolution time.

3.2. Influence of dissolution time on scaffold physico-chemical properties

3.2.1. Influence of dissolution time on the scaffold morphology

Figure 3a shows the histogram and **Figure 3b** the box-whisker plot of the fibre diameter distribution of the scaffolds obtained after 24, 48, 72 and 120 h of dissolution time in the hydrolytic acid solvent, as calculated from micrographs in **Figure 1**. The fibre diameter showed a decreasing tendency to lower values as dissolution time increased, from mean values of 125 nm

after 24 h to values around 95 nm after 120 h. Bead-free fibres were found after 24 and 48 h of dissolution time, while some beads in the microscale range were found for longer dissolution times (72 and 120 h). The diameter of these beads oscillated between 1.25 μm and 1.60 μm with concentrations of 9.75×10^{-2} and 9.16×10^{-2} beads $\cdot \mu\text{m}^{-2}$, for scaffolds prepared after 72 and 120 h respectively. These beads seem to be the responsible of the intense roughness observed at micrographs with lower magnification. According to bibliography, for a given concentration, the reduction of fibre diameter and the appearance of beads are usually related to a reduction of the solution viscosity due to the hydrolytic action of the solvent, and the subsequent lower incidence of chain entanglements [14] [44] [58].

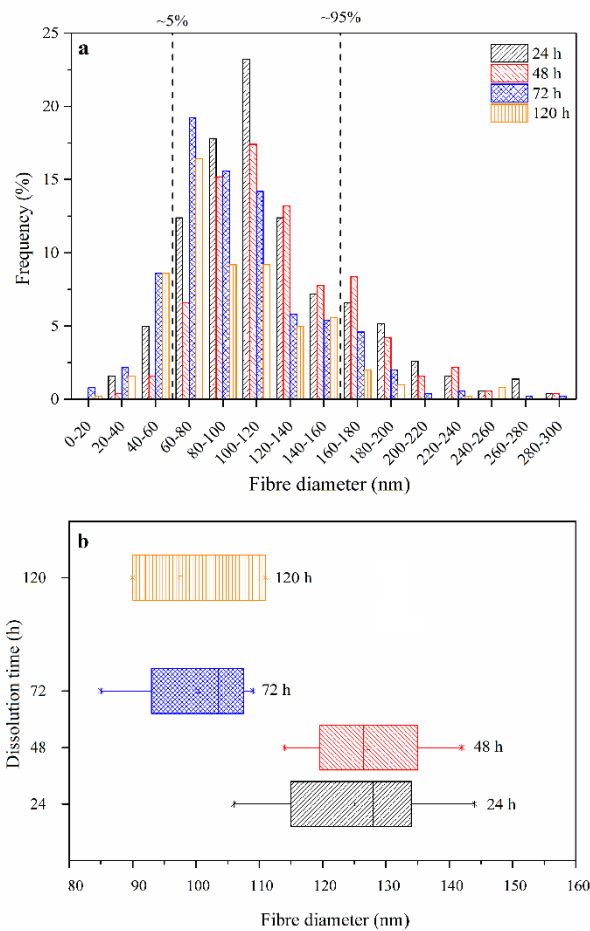


Figure 3. (a) Fibre diameter histogram for the scaffolds prepared after 24, 48, 72 and 120 h of dissolution. Dash lines indicate the approximated whisker limits (5 and 95%). (b) Box-whisker plots of the fibre diameter as a function of dissolution time. Box quartiles represent 25-75% and whiskers are between 5-95%.

3.2.2. Influence of dissolution time on the scaffold molar mass

The molar mass of the scaffolds was assessed by means of size exclusion chromatography (SEC) in terms of average molar mass in number (M_n), average molar mass in weight (M_w) and

polydispersity index (*PDI*), as shown in **Figure 4** for the pellet of PCL and electrospun scaffolds as a function of dissolution time in the hydrolytic acid solvent.

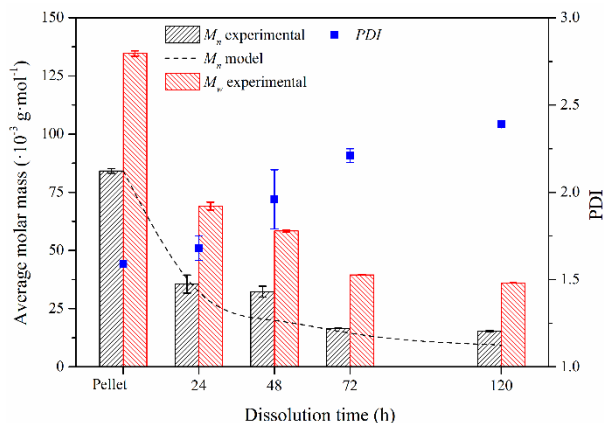


Figure 4. Average molar mass in number (M_n), average molar mass in weight (M_w) and polydispersity index (*PDI*) for PCL pellet, and electrospun scaffolds processed after 24, 48, 72 and 120 h of dissolution. Dotted line corresponds to the theoretical average molar mass in number values, as calculated from the method proposed by Lavielle et al. [44].

Overall, M_n decreased from 85000 to 15000 g·mol $^{-1}$, while M_w moved from 135000 to 36000 g·mol $^{-1}$ from the raw PCL (pellet) to the scaffold prepared after 120 h of solution preparation. As expected, the acidic nature of the solvent promoted a general decrease in the molar mass ascribed to the hydrolytic scission of the ester bond of PCL. The SEC analysis revealed that the chain scission of PCL was not linearly dependent on dissolution time: it was degraded faster at the early stage of solution preparation and tended to decrease slowly thereafter. Accordingly, an increase in the polydispersity index (*PDI*) was found from 1.59 to 2.39, which indicated the increase of cleavages of high molar mass segments, characteristic of a random chain scission according to the Flory's statistical theory [59]. All these results were in concordance with those obtained in other studies [43] [44]. In particular, a proper correlation (96% coincidence) between the expected theoretical –as calculated according to Lavielle et al. (**Supplementary Material**)– and the experimental values was obtained.

3.2.3. Influence of dissolution time on the scaffold microstructure

Fourier transformed infrared spectroscopy (FT-IR) was considered to perform a preliminary analysis of the change in the microstructure after electrospinning. **Figure 5a** shows the absorbance spectra in the 1100-1300 cm $^{-1}$ region for PCL pellet and electrospun scaffolds after 24, 48, 72 and 120 h of dissolution time in the hydrolytic acid solvent. It is well-known that, for polyesters, this spectral region appears to be the most sensitive to morphology differences, due to the appearance of C–C–H and O–C–H bending vibrations and C–C and C–O stretching vibrations [14] [60] [61]. Moreover, the bands located around 1162 and 1178 cm $^{-1}$ are related with

amorphous and crystalline morphology, respectively. The I_{1178}/I_{1162} intensity ratio is commonly used as an indicator of the change in the internal morphology of the fibres [14] [61]. **Figure 5b** shows a noticeable increase of crystallinity as a function of the dissolution time in the hydrolytic acid solvent up to 72 h, which remained from then onwards.

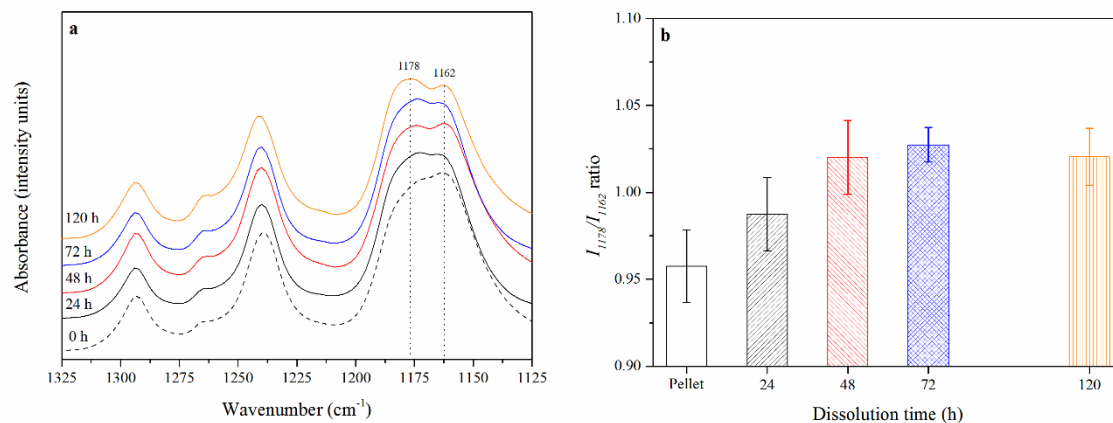


Figure 5. (a) FT-IR spectra in the 1325-1125 cm^{-1} region and (b) I_{1162}/I_{1178} ratio for PCL pellet, and electrospun scaffolds processed after 24, 48, 72 and 120 h of dissolution.

In order to corroborate these changes along the dissolution time, the differential scanning calorimetry (DSC) technique was used, which is considered to be adequate to understand the change in the microstructure of polymers subjected to a given degradation process [62] [63] [64] [65] [66] [67] [68]. The discussion in this section is given in terms of melting/crystallisation peak temperatures (T_{m1} , T_c , T_{m2}), lamellar thickness (l_{c1} , l_{c2}), specific enthalpies (Δh_{m1} , Δh_c , Δh_{m2}) and crystallinity degree (X_{c1} , X_{c2}), where subindexes 1 and 2 correspond to the 1st and 2nd heating scans, respectively. **Figure 6** plots the DSC thermograms of the 1st heating, cooling and 2nd heating scans for PCL pellet and scaffolds electrospun after 24, 48, 72 and 120 h of dissolution time in the hydrolytic acid solvent. Values of the main peak temperatures and enthalpies of the melting and crystallisation events are gathered in **Table 2**. The differences between melting enthalpies and peak temperatures obtained from the 1st and 2nd heating scans are explained by the different crystallisation behaviour of the PCL after electrospinning and differential scanning calorimetry. While electrospinning produces strain-induced crystallisation and was carried out at temperatures close to the T_c of the PCL [19] [69], the dynamic cooling of the DSC did not permit to achieve the same crystalline development [70].

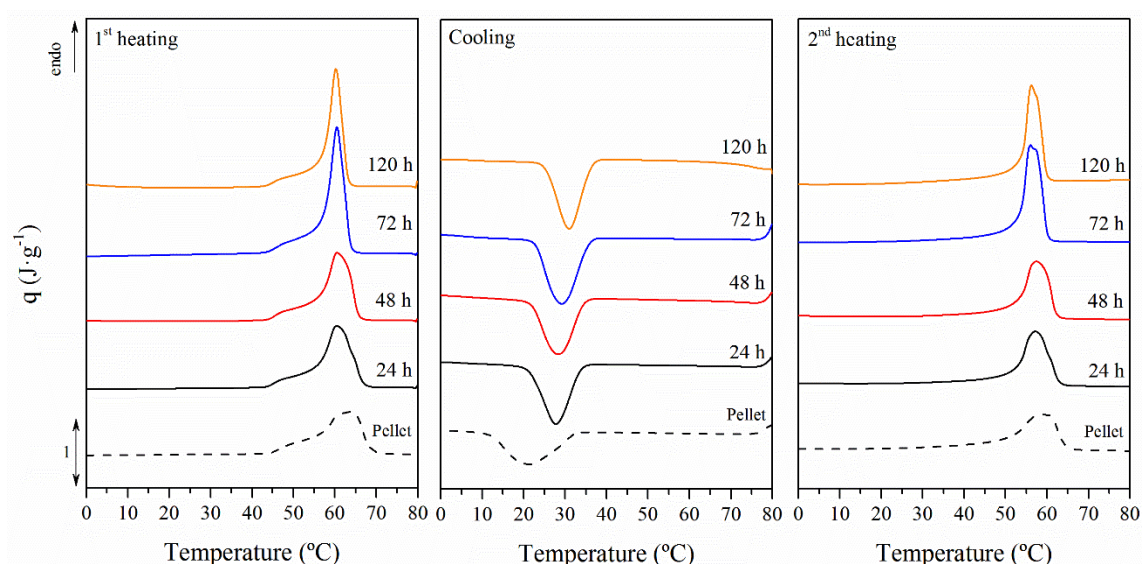


Figure 6. DSC traces of the 1st heating, cooling and 2nd heating scans for PCL pellet and scaffolds prepared after 24, 48, 72 and 120 h of dissolution.

Table 2. Melting enthalpy and temperature of the 1st heating scan (Δh_{m1} , T_{m1}), crystallisation enthalpy and temperature of the cooling scan (Δh_c , T_c) and melting enthalpy and temperature of the 2nd heating scan (Δh_{m2} , T_{m2}) as a function of the dissolution time for PCL pellet and scaffolds prepared after 24, 48, 72 and 120 h of dissolution time.

Dissolution time (h)	T_{m1} (°C)	Δh_{m1} (J·g ⁻¹)	T_c (°C)	Δh_c (J·g ⁻¹)	T_{m2} (°C)	Δh_{m2} (J·g ⁻¹)
PCL pellet	63.51 ± 1.27	45.60 ± 2.28	21.29 ± 0.43	-35.60 ± 1.78	59.70 ± 1.19	30.22 ± 1.51
24	61.78 ± 1.24	54.05 ± 3.22	27.40 ± 1.11	-40.45 ± 2.06	58.27 ± 1.09	39.67 ± 2.31
48	60.50 ± 1.21	52.34 ± 2.62	28.47 ± 0.57	-39.39 ± 1.97	57.53 ± 1.15	36.83 ± 1.84
72	60.63 ± 0.10	60.18 ± 1.80	29.96 ± 0.35	-44.89 ± 1.40	56.38 ± 0.30	44.22 ± 1.22
120	60.31 ± 0.12	58.39 ± 4.04	30.59 ± 0.49	-43.63 ± 2.68	56.87 ± 0.64	43.03 ± 2.93

In the 1st heating scan the melting peak is the result of at least two different melting transitions. A melting shoulder, placed at around 45 °C, seemed to remain constant, and can be ascribed to a crystalline population with a smaller lamellar thickness. The main melting peak, around 60 °C, is ascribed to the typical PCL melting behaviour, which sharpened and moved towards lower temperatures for a higher dissolution time in the hydrolytic acid solvent. During the cooling scan, a crystallisation transition occurred, which peak temperature (T_c) moved towards higher values from ~21 °C for PCL pellet to ~30 °C after 120 h of dissolution time. Since the changes in the T_c are closely related to the change in the molar mass of a polymer, the increase in the T_c corroborate the lower molar mass of the PCL scaffolds as the dissolution time increased. Shorter polymer chains which enhanced mobility crystallised at higher temperatures. Finally, in the 2nd heating scan, it was observed a melting peak located around 57 °C, which became sharper the longer the dissolution time was. With the purpose of deeply characterise the crystalline structure of the nanofibres, lamellar thickness distributions were calculated by applying the Thomson-Gibbs equation (**Equation 4**), based on the temperatures associated to the melting transitions [71] [72] [73] [74],

$$l_c(T_m) = \left[\left(1 - \frac{T_m}{T_m^0} \right) \cdot \frac{\Delta h_{mV}}{2 \cdot \sigma_e} \right]^{-1} \quad \text{(Equation 4)}$$

where T_m is the melting temperature; T_m^0 is the equilibrium melting temperature of an infinite crystal (348 K); σ_e is the surface free energy of the basal plane where the chains fold ($106 \cdot 10^{-3} \text{ J} \cdot \text{m}^{-2}$); and Δh_{mV} is the melting enthalpy per volume unit ($1.63 \cdot 10^8 \text{ J} \cdot \text{m}^{-3}$) [56]. **Figure 7a** shows the evolution of the lamellar thickness distributions for the 1st heating scan. PCL pellet showed a wide distribution, with a most probable lamellar thickness (l_c) around 45 nm. After electrospinning, narrower crystalline populations were obtained, showing a l_c around 32 nm. The promotion of smaller crystals ascribed to both the fast rate of solvent evaporation during electrospinning [46] [75] [76] and the stretching of shorter macromolecular chains [19], produced a more homogeneous crystalline structure. This observation was corroborated by the parameter defined as the full width at medium height of the lamellar thickness distributions ($FWMH$), which decreased with the dissolution time (**Figure 7b**).

With regards to the enthalpies for the aforementioned thermal transitions, in the 1st heating scan Δh_{m1} increased after electrospinning and even more as a function of dissolution time. Indeed, this tendency was perceived in the crystallinity degree (X_c), which ranged from 30.81% for PCL pellet to 36.52% and 40.66% for scaffolds prepared after 24 h and 120 h, respectively. Then, in the cooling scan, the Δh_c also increased with dissolution time, ranging from $-35.60 \text{ J} \cdot \text{g}^{-1}$ for PCL pellet to -40.45 and $-44.88 \text{ J} \cdot \text{g}^{-1}$ for electrospun samples after 24 h and 120 h, respectively. Consequently, as melting during the 2nd heating scan is directly related to the previous crystallisation during cooling, the tendency was also preserved. **Figure 7b** shows how the crystallinity degree (X_c) increased along with the aforementioned most probable lamellar thickness (l_c) and $FWMH$ reduction, which is ascribed to the homogenisation of the crystalline fraction.

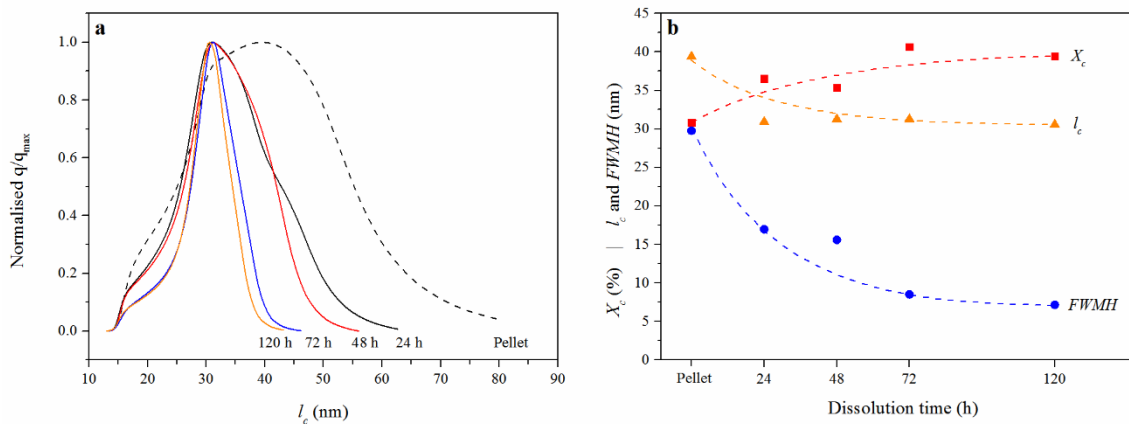


Figure 7. (a) Lamellar thickness distribution for PCL pellet and scaffolds prepared after 24, 48, 72 and 120 h of dissolution time as obtained in the 1st heating scan; (b) Crystallinity degree (X_c), most probable value of lamellar thickness (l_c) and value of full width at medium height ($FWMH$) as a function of dissolution time for PCL pellet and

scaffolds prepared after 24, 48, 72 and 120 h of dissolution as obtained from the 1st heating scan. Error bars were omitted for the sake of clarity (Error < 5%).

The most relevant results in this section can be inferred from the 1st scan, which showed the effects of the dissolution time and the electrospinning procedure. Although electrospinning is known to promote limited crystallisation by fast rate of solvent evaporation, the hydrolytic degradation of the PCL during dissolution promoted a reduction of the length of the polymeric chains, as observed in the previous section. Shorter molecular chains with enhanced mobility were more capable of forming crystalline domains than longer polymer chains due to the higher stretching, which enhanced crystallisation and orientation along the fibre axis [19]. In addition, more concise crystalline populations with smaller lamellar thickness were found as dissolution time increased.

3.3. *In vitro* validation of electrospun scaffolds

The *in vitro* behaviour of the electrospun PCL scaffolds was assessed by means of immersion in ultra-pure water and phosphate buffer solution (PBS), according to the international norm ISO 10993-13:2010-method 4.3 [57]. The validation procedure extent was established to 100 days, which was considered as a reasonable time-span to evaluate physico-chemical changes along their hypothetical service life.

A qualitative and visual analysis of the changes in the surface morphology after the validation procedure is shown in **Figure 8**, whereas the quantification of those changes by means of the fibre diameter evaluation is shown in **Figure 9**. Then the variations of the mass, the pH of the degradation media, the molar mass, the crystallinity degree and the lamellar thickness are plotted in **Figure 10**.

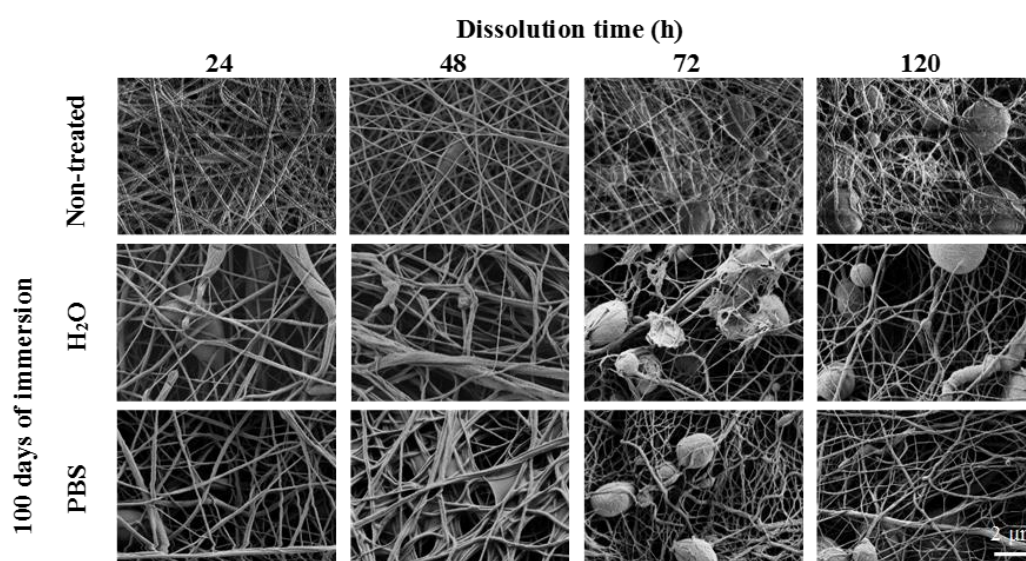


Figure 8. Fibre surface morphology (10000 \times , 3kV) as a function of dissolution time for PCL scaffolds prior to and after 100 days of immersion in ultra-pure water and PBS.

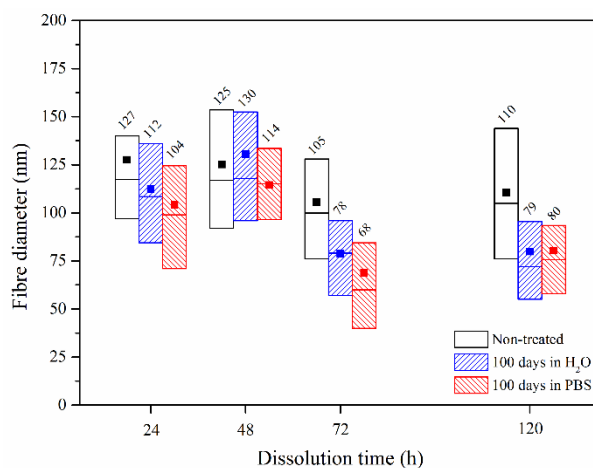


Figure 9. Box plot of the fibre diameter as a function of the dissolution time for PCL scaffolds prior to and after 100 days of immersion in ultra-pure water and PBS. Solid squares stand for the averages while the upper, middle and lower limits correspond to the first, second and third quartiles (75%, 50% and 25%, respectively).

Apparently, the original nanofibrous structure seemed to remain unaffected after 100 days of immersion in both water and PBS media. Erosion at this stage was not significant enough to be appreciated from the fibre appearance, but a deep assessment of the fibre diameter showed two differentiated behaviours. As shown in **Figure 10**, the scaffolds prepared after 24 h and 48 h practically kept their fibre diameter distributions after immersion. However, the diameter reduction was found to be noticeable as dissolution time increased. The scaffolds prepared after 72 h and 120 h showed a significant reduction (30–40%) of the fibre diameter after 100 days of *in vitro* validation. A similar behaviour was found in water and PBS, but a scarcely greater diameter decrease was observed in the buffered solution. Although the samples were vacuum dried before analysis, this performance could be ascribed to the higher fibre swelling due to the water absorption, compared to the lower PBS penetration.

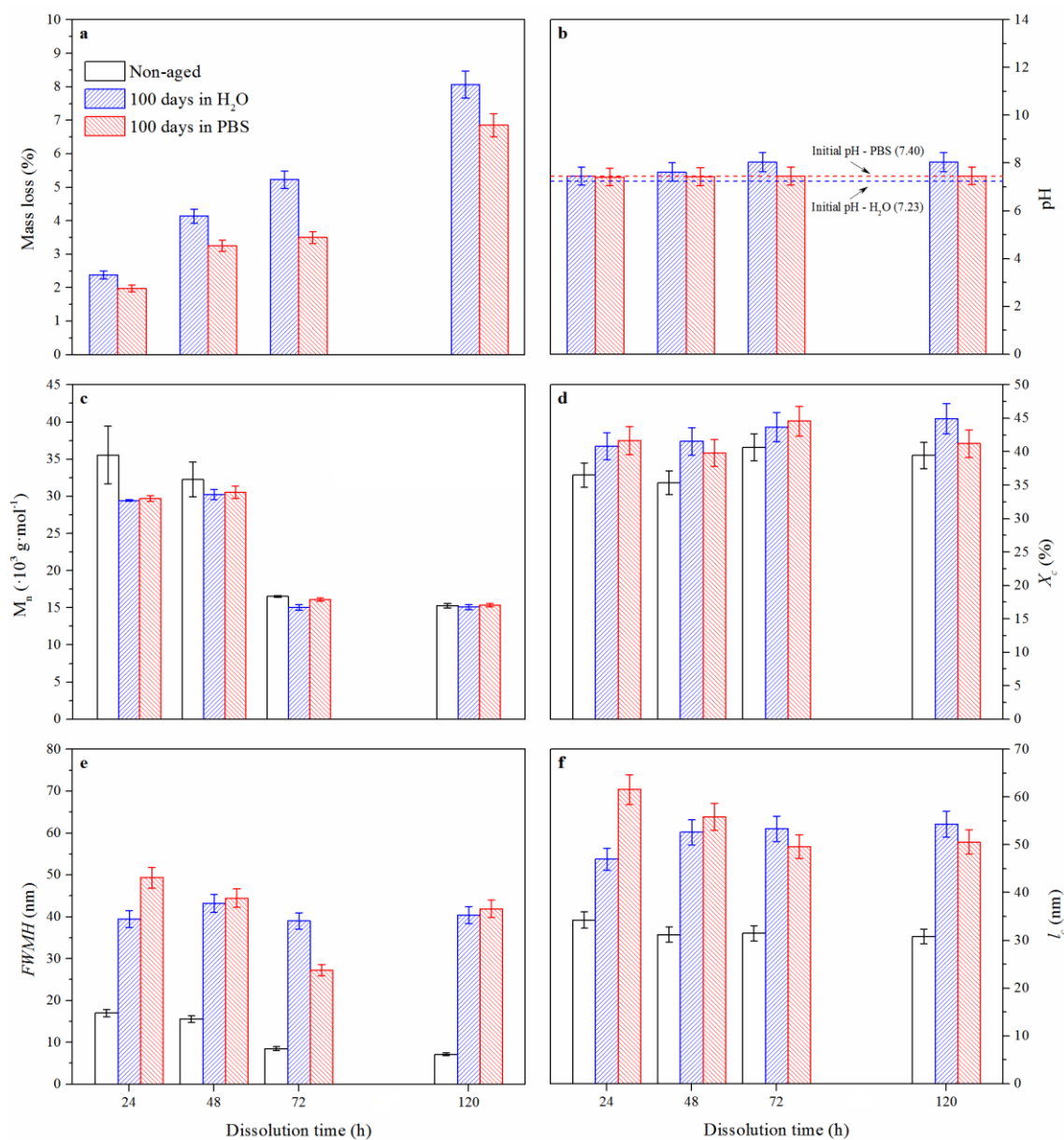


Figure 10. Evolution of several parameters selected as indicators for the assessment of the hydrolytic degradation after 100 days of immersion in aqueous and PBS media of the electrospun scaffolds processed after 24, 48, 72 and 120 h of dissolution time: **(a)** Mass loss; **(b)** pH of the media; **(c)** Average molar mass in number (M_n); **(d)** Crystallinity degree (X_c); **(e)** Full width at medium height of the lamellar thickness distribution (FWMH); and **(f)** Peak of the lamellar thickness distribution (l_c).

Erosion results as obtained by **Equation 2** are plotted in **Figure 10a**. Greater mass loss was found as a function of dissolution time, which is related to the diffusion of higher amount of oligomeric species to the biodegradation media of greatly degraded scaffolds [77]. Slightly greater mass loss in water than in PBS for a given dissolution time was perceived. This difference can be ascribed to the capability of the PBS to buffer released acidic low molar mass compounds, avoiding autocatalytic degradation and thus, retarding the erosion process.

The changes on the molar mass and the fibre microstructure were subsequently assessed. **Figure 10c** shows the average molar mass in number (M_n), which decreased more the lower the dissolution time was. Since the hydrolytic degradation is known to take place mainly in the amorphous regions of the samples, those with lower initial crystallinity degree showed higher molar mass reduction (scaffolds electrospun after 24 and 48 h) [78] [79]. Conversely, a greater initial crystallinity degree along with the growth of the lamellar thickness during immersion, prevented the scaffolds from hydrolytic degradation [80] [81] (scaffolds electrospun after 72 and 120 h).

Interestingly, the effect of the *in vitro* validation procedure after 100 days was relevant in terms of development of chemically-induced crystallisation [65] [67] [80], as plotted in **Figures 10d**, **10e** and **10f**, but not in the molar mass which barely changed for all studied scaffolds. Indeed, crystallisation was driven by the combination of water and temperature. Water acted both as plasticizer to permit the mobility of polymer segments and promoted chain scission and mass loss. In addition, the temperature of the *in vitro* validation at 37 °C was close to the crystallisation temperature of PCL, as shown in **Table 2**. Therefore, there was a widening of the lamellar thickness distribution, an increase of its peak value and subsequent increase of the crystallinity degree, being more relevant the higher the dissolution time during the preparation of the scaffolds was.

Overall, the PCL based structure remained almost unaffected in the nanoscale range after the *in vitro* evaluation, which is essential for long-term biomedical applications, when no-collapsing structures are needed [83, 84, 85]. This behaviour was supported by the development of chemically-induced crystallisation, that reduced the amorphous/crystalline proportion and prevented the scaffold from hydrolytic degradation, as observed by the slightly modification of the molar mass.

4. Conclusions

Nanofibrous scaffolds were obtained by electrospinning of polycaprolactone (PCL) in 1:1 formic/acetic acid solvent. When viable, a non-significant influence of the voltage and feeding rate was found on the fibre diameters of scaffolds, while the influence of the dissolution time in the hydrolytic acid solvent was found to play a key role in the resultant physico-chemical properties, morphology and *in vitro* performance of the electrospun scaffolds.

The chain scission of PCL occurred through the hydrolytic degradation of the ester bonds along the dissolution preparation prior to electrospinning. The hydrolytic acid solvent reduced the molar mass of the electrospun scaffolds, increased the crystallinity degree and slightly lowered the lamellar thickness. Bead-free fibres were obtained after 24 h and 48 h of dissolution. Particularly

at longer dissolution times (72 h and 120 h), an intense reduction of molar mass and fibre diameter along with the apparition of beads was revealed.

The *in vitro* behaviour of the scaffolds after 100 days of immersion in water and PBS revealed some differences depending on the dissolution time prior to electrospinning. However, for all the scaffolds, the nanoscaled structure remained almost unaffected after the *in vitro* evaluation. This behaviour was supported by the development of chemically-induced crystallisation, that reduced the amorphous/crystalline proportion and prevented the scaffold from hydrolytic degradation, as observed by the slightly modification of the molar mass.

This tailoring procedure permitted to obtain scaffolds that maintained the nanoscaled structure after such long *in vitro* evaluation. This is essential for long-term PCL-based patches, when non-collapsing structures are needed. Future investigations will open up the possibility of functionalising this scaffolds with other components and studying the differentiation ability of cells onto these devices, as well as studying their biodegradation behaviour when implanted *in vivo*.

Acknowledgements

The Spanish Ministry of Economy and Competitiveness is acknowledged for the projects POLYCELL (ENE2014-53734-C2-1-R) and UPOV13-3E-1947. The Spanish Ministry of Education, Culture and Sports is thanked for the pre-doctoral FPU grant of O. Gil-Castell (FPU13/01916) and the scholarship for a research stage of O. Gil-Castell in Kungliga Tekniska Högskolan (KTH). Generalitat Valenciana is thanked for the APOSTD/2014/041 for J.D. Badia. Universitat de València (UV) and IIS LaFe are acknowledged for the DERMASAFE project. The financial support given by the KTH Royal Institute of Technology is gratefully acknowledged. IESMAT S.A. and Malvern Instruments Ltd are recognised for their grateful collaboration.

References


- [1] Coland ED, Matthews JA, Pawlowski KJ, Sompson DG, Wnek GE, Gary L. Electrospinning collagen and elastin: preliminary vascular tissue engineering. *Frontiers in Bioscience* 2004;9:1432-1442.
- [2] Ma ZW, Kotaki M, Inai R, Ramakrishna S. Potential of nanofiber matrix as tissue-engineering scaffolds. *Tissue Engineering* 2005;11(1-2):101-109.
- [3] Agarwal S, Greiner A, Wendorff JH. Functional materials by electrospinning of polymers. *Progress in Polymer Science* 2013;38:963-991.
- [4] Xu CY, Inai R, Kotaki M, Ramakrishna S. Aligned biodegradable nanofibrous structure: a potential scaffold for blood vessel engineering. *Biomaterials* 2004;25:877-886.
- [5] Ma PX. Scaffolds for tissue fabrication. *Materials Today* 2004;7:30-40.
- [6] Smith LA, Ma PX. Nano-fibrous scaffolds for tissue engineering. *Colloids and Surfaces B: Biointerfaces* 2004;39:125-131.
- [7] Buttafoco L, Kolkman NG, Engbers-Buijtenhuijs P, Poot AA, Dijkstra PJ, Vermes I, Feijen J. Electrospinning of collagen and elastin for tissue engineering applications. *Biomaterials* 2006;27:724-734.
- [8] Zhang Y, Ouyang H, Lim CT, Ramakrishna S, Huang ZM. Electrospinning of gelatin fibers and gelatin/PCL composite fibrous scaffolds. *Journal of Biomedical Materials Research, Part B: Applied Biomaterials* 2005;72B:156-165.
- [9] Pham Q, Sharma U, Mikos A. Electrospinning of polymeric nanofibers for tissue engineering applications: a review. *Tissue Engineering* 2006;12:1197-1211.
- [10] Zong X, Kim K, Fang D, Ran S, Hsiao B, Chu B. Structure and process relationship of electrospun bioabsorbable nanofiber membranes. *Polymer* 2002;43:4403-4412.
- [11] Zeng J, Chen X, Xu X, Liang Q, Bian X, Yang L, et al. Ultrafine fibers electrospun from biodegradable polymers. *Journal of Applied Polymer Science* 2003;89:1085-1092.
- [12] Yarin AL, Koombhongse S, Reneker DH. Bending instability in electrospinning of nanofibers. *Journal of Applied Physics* 2001;90:4836-4846.
- [13] Deitzel JM, Kleinmeyer J, Harris D, Beck Tan NC. The effect of processing variables on the morphology of electrospun anofibers and textiles. *Polymer* 2001;42:261-272.
- [14] Guarino V, Cirillo V, Taddei P, Alvarez-Perez MA, Ambrosio L. Tuning size scale and crystallinity of PCL electrospun fibres via solvent permittivity to address hMSC Response. *Macromolecular Bioscience* 2011;11:1694-1705.
- [15] Chong EJ, Phan TT, Lim IJ, Zhang YZ, Bay BH, Ramakrishna S, et al. Evaluation of electrospun PCL/gelatin nanofibrous scaffold for wound healing and layered dermal reconstitution. *Acta Biomaterialia* 2007;3:321-330.
- [16] Agarwal S, Wendorff JH, Greiner A. Use of electrospinning technique for biomedical applications. *Polymer* 2008; 49(26):5603-5621.
- [17] Nepalli R, Marega, Margi A, Bajgai MP, Kim HY, Causin V. Poly(epsilon-caprolactone) filled with electrospun nylon fibres: a model for a facile composite fabrication. *European Polymer Journal* 2010;46(5):968-976.
- [18] Venugopal J, Zhang YZ, Ramakrishna S. Fabrication of modified and functionalized polycaprolactone nanofiber scaffolds for vascular tissue engineering. *Nanotechnology* 2005;16(10):2138-2142.
- [19] Wang X, Zhao H, Turng LS, Li Q. Crystalline morphology of electrospun poly(epsilon-caprolactone) (PCL) nanofibers. *Industrial and Engineering Chemistry Research* 2013;52:4939-4949.
- [20] Jha BS, Colello RJ, Bowman JR, Sell SA, Lee KD, Bigbee JW, Bowlin GL, Chow WN, Mathern BE, Simpson DG. Two pole air gap electrospinning: fabrication of highly aligned, three-dimensional scaffolds for nerve reconstruction. *Acta Biomaterialia* 2011;, 7(1):203-215.
- [21] Ghasemi-Mobarakeh L, Prabhakaran MP, Morshed M, Nasr-Esfahani M-H, Ramakrishna S. Electrospun poly(e-caprolactone)/gelatin nanofibrous scaffolds for nerve tissue engineering. *Biomaterials* 2008;29(34):4532-4539.
- [22] Bosworth L, Clegg P, Downes S. Electrospun nanofibres of polycaprolactone, and their use for tendon regeneration. *International Journal of Nano and Biomaterials* 2008;1(3):263-279.

- [23] Zamarripa N, Farboodmanesh S, Kuo CK. Novel biomimetic scaffold for tendon and ligament tissue engineering. Bioengineering conference, 2009 IEEE 35th annual northeast.
- [24] Powell HM, Boyce ST. Engineered human skin fabricated using electrospun collagen-PCL blends: morphogenesis and mechanical properties. *Tissue Engineering Part A* 2009;15(8):2177–2187.
- [25] Chen H, Huang J, Yu J, Liu S, Gu P. Electrospun chitosan graft-poly (ε-caprolactone)/poly (ε-caprolactone) cationic nanofibrous mats as potential scaffolds for skin tissue engineering. *International Journal of Biological Macromolecules* 2011;48(1):13–19.
- [26] Lee KH, Kim HY, Khil MS, Ra YM, Lee DR. Characterization of nanostructured poly(ε-caprolactone) nonwoven mats via electrospinning. *Polymer* 2003;44(4):1287–1294.
- [27] Duan Y, Jia J, Wang S, Yan W, Jin L, Wang Z. Preparation of antimicrobial poly(ε-caprolactone) electrospun nanofibers containing silver-loaded zirconium phosphate nanoparticles. *Journal of Applied Polymer Science* 2007;106(2):1208–1214.
- [28] Moghe AK, Hufenus R, Hudson SM, Gupta BS. Effect of the addition of a fugitive salt on electrospinnability of poly(ε-caprolactone). *Polymer* 2009;50(14):3311–8.
- [29] Lowery JL, Datta N, Rutledge GC. Effect of fiber diameter, pore size and seeding method on growth of human dermal fibroblasts in electrospun poly(ε-caprolactone) fibrous mats. *Biomaterials* 2010;31(3):491–504.
- [30] Del Gaudio C, Grigioni M, Bianco A, De Angelis G. Electrospun bioresorbable heart valve scaffold for tissue engineering. *International Journal of Artificial Organs* 2008;31(1):68–75.
- [31] Li W, Tuli R, Okafor C, Derfoul A, Danielson KG, Hall DJ, et al. A three-dimensional nanofibrous scaffold for cartilage tissue engineering using human mesenchymal stem cells. *Biomaterials* 2005;26(6):599–609.
- [32] Shin M, Ishii O, Sueda T, Vacanti JP. Contractile cardiac grafts using a novel nanofibrous mesh. *Biomaterials* 2004;25(17):3717–3723.
- [33] Gaumer J, Prasad A, Lee D, Lannutti J. Structure-function relationships and source-to-ground distance in electrospun polycaprolactone. *Acta Biomaterialia* 2009;5(5):1552–1561.
- [34] Del Gaudio C, Bianco A, Folin M, Baiguera S, Grigioni M. Structural characterization and cell response evaluation of electrospun PCL membranes: micrometric versus submicrometric fibers. *Journal of Biomedical Materials Research A* 2009;89A(4):1028–1039.
- [35] Yu H, Jang J, Kim T, Lee H, Kim H. Apatite-mineralized polycaprolactone nanofibrous web as a bone tissue regeneration substrate. *Journal of Biomedical Material Research A* 2009;88A(3):747–754.
- [36] Li X, Xie J, Yuan X, Xia Y. Coating electrospun poly(ε-caprolactone) fibers with gelatin and calcium phosphate and their use as biomimetic scaffolds for bone tissue engineering. *Langmuir* 2008;24(24):14145–14150.
- [37] Eriskin C, Kalyon DM, Wang H. Functionally graded electrospun polycaprolactone and b-tricalcium phosphate nanocomposites for tissue engineering applications. *Biomaterials* 2008;29(30):4065–4073.
- [38] Yang F, Wolke JGC, Jansen JA. Biomimetic calcium phosphate coating on electrospun poly(ε-caprolactone) scaffolds for bone tissue engineering. *Chemical Engineering Journal* 2008;137(1):154–161.
- [39] Nam J, Huang Y, Agarwal S, Lannutti J. Materials selection and residual solvent retention in biodegradable electrospun fibers. *Journal of Applied Polymer Science* 2008;107(3):1547–1554.
- [40] Browning E. Toxic solvents: a review. *British Journal of Industrial Medicine* 1959;16(1):23–39.
- [41] Bosworth LA, Downes S. Acetone, a sustainable solvent for electrospinning poly(ε-caprolactone) fibres: effect of varying parameters and solution concentrations on fibre diameter. *Journal of Polymers and the Environment* 2012;20:879–886.
- [42] Bisnual NS, Natarajan A, Menon D, Bhaskaran VK, Mony U, Nair SV. PCL-gelatin composite nanofibers electrospun using diluted acetic acid-ethyl acetate solvent system for stem cell-based bone tissue engineering. *Journal of Biomaterials Science, Polymer Edition*, 2014;25(4):325–340.
- [43] Van der Schueren L, De Schoenmaker B, Kalaoglu OI, De Clerck K. An alternative solvent system for the steady state electrospinning of polycaprolactone. *European Polymer Journal* 2011;47:1256–1263.

- [44] Lavielle N, Popa AM, de Geus M, Hébraud A, Schlatter G, Thöny-Meyer L, Rossi RM. Controlled formation of poly(ϵ -caprolactone) ultrathin electrospun nanofibers in a hydrolytic degradation-assisted process. *European Polymer Journal* 2013;49:1331-1336.
- [45] Pereira IH, Ayres E, Averous L, Schlatter G, Hebraud A, Mendes STOL, Oréface RL. Elaboration and characterization of coaxial electrospun poly(ϵ -caprolactone)/gelatin nanofibers for biomedical applications. *Advances in Polymer Technology*, 2014;33:21475.
- [46] Griffith LG. Polymeric biomaterials. *Acta Materialia*, 2000;48:263.
- [47] Aharoni Sm. Increased glass transition temperature in motionally constrained semi crystalline polymers. *Polmer for Advanced Technologies*, 1998;9:169.
- [48] Chen DR, Bei JZ, Wang SG. Polycaprolactone microparticles and their biodegradation. *Journal of Polymer Degradation and Stability*, 2000;67:455.
- [49] Jenkins MJ, Harrison KL. The effect of crystalline morphology on the degradation of polycaprolactone in a solution of phosphate buffer and lipase. *Polymers for Advanced Technologies*, 2008;19:1901-1906.
- [50] Mark JE. *Physical Properties of Polymers Handbook*, Springer, 2007. p 636.
- [51] Hamley IW. Structure and flow behaviour of block copolymers. *Journal of Physics: Condensed Matter*, 2001;13:643-671.
- [52] Thomas EL, Anderson DM, Henkee CS. Periodic area-minimizing surfaces in block copolymers. *Nature*, 1988;334:598-601.
- [53] Suzuki Y, Duran H, Akram W, Steinhart M, Floudas G, Butt HJ. Multiple nucleation events and local dynamics of poly(ϵ -caprolactone) (PCL) confined to nanoporous alumina. *Soft Matter* 2013;9:9189-9198.
- [54] ISO10993-13:2010 Biological evaluation of medical devices - Part 13: Identification and quantification of degradation products from polymeric medical devices.
- [55] Fong H, Chun I, Reneker DH. Beaded nanofibers formed during electrospinning. *Polymer* 1999;40(16):4585-92.
- [56] Yu H, Huang N, Wang C, Tang Z. Modeling of poly(L-lactide) thermal degradation: theoretical prediction of molecular weight and polydispersity index. *Journal of Applied Polymer Science* 2003;88(11):2557-2562.
- [57] Snyder Rg, Maroncelli M, Strauss HL, Hallmark VL. Temperature and phase behaviour of infrared intensities: the poly(methylene) chain. *The Journal of Physical Chemistry* 1986;90:5263-5630.
- [58] Coleman MM, Zarina J. Fourier-transform infrared studies of polymer blends. II. Poly(ϵ -caprolactone)-poly(vinyl chloride) system. *Journal of Polymer Science: Polymer Physics Edition* 1979;17(5):837-850.
- [59] Badia JD, Vilaplana F, Karlsson S, Ribes-Greus A. Thermal analysis as a quality tool for assessing the influence of thermo-mechanical degradation on recycled poly(ethylene terephthalate). *Polymer Testing* 2009;28(2):169-75.
- [60] Santonja-Blasco L, Moriana R, Badía JD, Ribes-Greus A. Thermal analysis applied to the characterization of degradation in soil of polylactide: I. calorimetric and viscoelastic analyses. *Polymer Degradation and Stability* 2010;95(11):2192-9.
- [61] Badia JD, Strömberg E, Karlsson S, Ribes-Greus A. Material valorisation of amorphous polylactide. Influence of thermo-mechanical degradation on the morphology, segmental dynamics, thermal and mechanical performance. *Polymer Degradation and Stability* 2012;, 97(4):670-8.
- [62] Badia JD, Santonja-Blasco L, Martínez-Felipe A, Ribes-Greus A. Hygrothermal ageing of reprocessed polylactide. *Polymer Degradation and Stability* 2012;97(10):1881-90.
- [63] Badia JD, Strömberg E, Karlsson S, Ribes-Greus A. The role of crystalline, mobile amorphous and rigid amorphous fractions in the performance of recycled poly (ethylene terephthalate) (PET). *Polymer Degradation and Stability* 2012;97(1):98-107.
- [64] Gil-Castell O, Badia JD, Kittikorn T, Strömberg E, Martínez-Felipe A, Ek M, Karlsson S, Ribes-Greus A. Hydrothermal ageing of polylactide/sisal biocomposites. Studies of water absorption behaviour and Physico-Chemical performance., *Polymer Degradation and Stability* 2014;108:212-222.
- [65] Badia JD, Kittikorn T, Strömberg E, Santonja-Blasco L, Martínez-Felipe A, Ribes-Greus A, Ek M, Karlsson S. Water absorption and hydrothermal performance of PHBV/sisal biocomposites. *Polymer Degradation and Stability* 2014;108:166-174.

- [66] Kimura N, Kim HK, Kim BS, Lee KH, Kim IS. Molecular orientation and crystalline structure of aligned electrospun nylon-6 nanofibers: Effect of gap size. *Macromolecular Materials and Engineering* 2010;295:1090-1096.
- [67] Zhuravlev E, Schmelzer JWP, Wunderlich B, Schick C. Kinetics of nucleation and crystallization in poly(ϵ -caprolactone) (PCL). *Polymer* 2011;52(9):1983-1997.
- [68] Lauritzen JL, Hoffman JD. Theory of formation of polymer crystals with folded chains in dilute solution. *Journal of Research of the National Bureau of Standards* 1960;64:73-102.
- [69] Lauritzen JL, Hoffman JD. Crystallization of bulk polymers with chain folding: theory of growth of lamellar spherulites. *Journal of Research of the National Bureau of Standards* 1961;65:297-336.
- [70] Hoffman JD, Davis GT, Lauritzen JL. In: Hannay NB, editor. *Crystalline and noncrystalline solids*, vol. 3. New York: Plenum Press; 1976.
- [71] Gil-Castell O, Badia JD, Teruel-Juanes R, Rodriguez I, Meseguer F, Ribes-Greus A. Novel Silicon microparticles to improve sunlight stability of raw polypropylene. *European Polymer Journal* 2015;70:247-261.
- [72] Arinstein A, Burman M, Gendelman O, Zussman E. Effect of supramolecular structure on polymer nanofibre elasticity. *Nature Nanotechnology* 2007;2:59-62.
- [73] Hohmann MM, Shin M, Rutledge G, Brenner MP. Electrospinning and electrically forced jets I stability theory. *Physics of fluids* 2001;13(8):2201-2220.
- [74] Kolbuk D, Sajkiewicz P, Maniura-Weber K, Fortunato G. Structure and morphology of electrospun polycaprolactone/gelatine nanofibers. *European Polymer Journal* 2013;49:2052-2061.
- [75] Rutkowska M, Jasterzebska M, Janik H. Biodegradation of polycaprolactone in seawater. *Reactive and Functional Polymers*, 1998;38:27.
- [76] Hakkarainen M, Albertsson AC, Karlsson S. Weight losses and molecular weight changes correlated with the evolution of hydroxyacids in simulated in vivo degradation of homo- and copolymers of PLA and PGA. *Polymer Degradation and Stability* 1996, 52(3):283-291.
- [77] Vert M, Li SM, Garreau H. Attempts to map the structure and degradation characteristics of aliphatic polyesters derived from lactic and glycolic acids. *Journal of Biomaterial Science. Polymer Edition* 1994;6(7):639-649.
- [78] Li SM, Garreau H, Vert M. Structure-property relationships in the case of the degradation of massive aliphatic poly(α -hydroxyacids) in aqueous media. Part 3: influence of the morphology of poly(L-lactic acid). *Journal of Materials Science, Materials in Medicine* 1990;1:198-206.
- [79] Antheunis H, van der Meer JC, de Geus M, Kingma W, Koning CE. Improved mathematical model for the hydrolytic degradation of aliphatic polyesters. *Macromolecules* 2009;42:2462-2471.
- [80] Gil-Castell O, Badia JD, Kittikorn T, Strömberg E, Ek M, Karlsson S, Ribes-Greus A. Impact of hydrothermal ageing on the thermal stability, morphology and viscoelastic performance of PLA/sisal biocomposites. *Polymer Degradation and Stability* 2016, 132:87-96.
- [81] Tillman BW, Yazdani SK, Lee SJ, Geary RL, Atala A, Yoo JJ. The in vivo stability of electrospun polycaprolactone-collagen scaffolds in vascular reconstruction. *Biomaterials* 2009;30(4):583-588.
- [82] Hakimi O, Mouthuy PA, Carr A. Synthetic and degradable patches: an emerging solution for rotator cuff repair. *International Journal of Experimental Pathology*, 2013;94(4):287-292.
- [83] Fujimoto KL, Guan J, Oshima H, Sakai T, Wagner W. In vivo evaluation of a porous, elastic, biodegradable patch for reconstructive cardiac procedures. *The annals of Thoracic Surgery*, 2007;83(2):648-654.
- [84] Cai H, Dave V, Gross RA, McCarthy SP. Effects of physical aging, crystallinity, and orientation on the enzymatic degradation of poly(lactic acid). *Journal of Polymer Science Part B: Polymer Physics*, 1996;34(16):2701-2708.
- [85] Pantani R, Sorrentino A. Influence of crystallinity on the biodegradation rate of injection-moulded poly(lactic acid) samples in controlled composting conditions. *Polymer Degradation and Stability*, 2013;98:1089-1096.

ANNEX – OPEN ACCESS POLICIES


... opening access to research

Home • Search • Journals • Publishers • FAQ • Suggest • About
English | Español | Magyar | Nederlands | Português

Search - Publisher copyright policies & self-archiving

One journal found when searched for: 0014-3057

Journal: European Polymer Journal (ISSN: 0014-3057)
RoMEO: This is a RoMEO: green journal
Paid OA: A paid open access option is available for this journal.
Author's Pre-print: ✓ author can archive pre-print (ie pre-refereeing) Author's Post-print: ✓ author can archive post-print (ie final draft post-refereeing) Publisher's Version/PDF: ✗ author cannot archive publisher's version/PDF
General Conditions: <ul style="list-style-type: none"> Authors pre-print on any website, including arXiv and RePEc Author's post-print on author's personal website immediately Author's post-print on open access repository after an embargo period of between 12 months and 48 months Permitted deposit due to Funding Body, institutional and Governmental policy or mandate, may be required to comply with embargo periods of 12 months to 48 months Author's post-print may be used to update arXiv and RePEc Publisher's version/PDF cannot be used Must link to publisher version with DOI Author's post-print must be released with a Creative Commons Attribution Non-Commercial No Derivatives License
Mandated OA: (Awaiting information)
Paid Open Access: Open Access
Notes: <ul style="list-style-type: none"> Publisher last reviewed on 03/06/2015
Copyright: Unleashing the power of academic sharing - Sharing Policy - Sharing and Hosting Policy FAQ - Green open access - Journal Embargo Period List (pdf) - Journal Embargo List for UK Authors - Attaching a User License (pdf) - Funding Body Agreements
Updated: 01-May-2015 - Suggest an update for this record
Link to this page: http://www.sherpa.ac.uk/romeo/issn/0014-3057/
Published by: Elsevier - Green Policies in RoMEO

This summary is for the journal's default policies, and changes or exceptions can often be negotiated by authors.
All information is correct to the best of our knowledge but should not be relied upon for legal advice.